



Pergamon

*J. Mech. Phys. Solids*, Vol. 46, No. 10, pp. 1789–1813, 1998

© 1998 Elsevier Science Ltd. All rights reserved

Printed in Great Britain

0022-5096/98 \$—see front matter

PII: S0022-5096(98)00036-2

## INTERSONIC CRACK PROPAGATION IN BIMATERIAL SYSTEMS

ARES J. ROSAKIS,\*<sup>a</sup> OMPRAKASH SAMUDRALA,<sup>a</sup> RAMAN P. SINGH<sup>a</sup>  
and A. SHUKLA<sup>b</sup>

<sup>a</sup> Graduate Aeronautical Laboratories, California Institute of Technology, Pasadena CA 91125, U.S.A.; <sup>b</sup> Department of Mechanical Engineering, University of Rhode Island, Kingston, RI 02881, U.S.A.

(Received 20 December 1997; in revised form 13 February 1998)

### ABSTRACT

This paper describes experimental observations of various phenomena characteristic of dynamic intersonic decohesion of bimaterial interfaces. Two separate but complementary optical methods are used in conjunction with high-speed photography to explore the nature of the large-scale contact and mach wave formation at the vicinity of running cracks in two different bimaterial systems. Theoretical predictions of crack tip speed regimes, where large-scale contact is implied, are confirmed. Also, the theoretically predicted mach wave emanating from the intersonically propagating crack tip is observed. Direct visual evidence is also obtained for another traveling mach wave emanating from the end of the intersonically moving contact zone. Subsequently, a physical model for intersonic crack propagation along bimaterial interfaces is presented and ratified in view of recent experimental observations and theoretical developments. Finally, the paper presents very recent experimental evidence that shows crack tip speeds exceeding the intersonic regime and becoming clearly supersonic. © 1998 Elsevier Science Ltd. All rights reserved.

Keywords: A. dynamic fracture, B. crack mechanics, layered material, D. optical interferometry.

### INTRODUCTION

In homogeneous materials, the observations of crack growth speeds greater than the shear wave speed,  $v > c_s$ , is limited to the cases when the loading is applied directly to the propagating crack tip. For remotely loaded cracks, energy considerations make it impossible for the crack tip speed to exceed the Rayleigh wave speed of the material (Broberg, 1960; Freund, 1990). Thus, the only experimental observations of intersonic or supersonic crack tip speeds,  $v > c_s$  or  $v > c_r$ , in a laboratory setting have been on crack growth along weak crystal planes in single crystals of potassium chloride, where the crack faces were loaded by laser induced expanding plasma (Winkler *et al.*, 1970; Curran *et al.*, 1970). Indirect observation of intersonic shear rupture ( $c_s < v < c_r$ ) has also been reported for crustal earthquakes (Archuleta, 1982). These observations have motivated extensive theoretical work in the area of high-speed shear fracture in homogeneous materials. This has been primarily conducted with seismological

\* To whom correspondence should be addressed. Tel.: 626 395 3690. Fax: 626 449 2677. E-mail: rosakis@atlantis.caltech.edu

applications in mind and includes the work of Burrige (1973), Burrige *et al.* (1979), Freund (1979), Broberg (1985, 1989), Georgiadis (1986), Bykovtsev and Kramarovskii (1989) and Aleksandrov and Smetanin (1990).

In bimaterial systems, however, it has been recently demonstrated (by the authors and their coworkers) that intersonic crack propagation along bimaterial interfaces is possible even under remote loading conditions (Liu *et al.*, 1993; Lambros and Rosakis, 1995a, b, c; Singh and Shukla, 1996). Indeed, it has been experimentally shown that if there exists a significant mismatch in the stress wave speeds across the bimaterial interface then the crack can propagate intersonically with respect to the material with the lower shear wave speed, while it remains subsonic with respect to the material with the higher wave speed. Under these conditions only a finite amount of energy has to be supplied to the crack tip to maintain extension as the propagational speed approaches the lower of the two Rayleigh wave speeds. This fact was analytically confirmed by Yang *et al.* (1991) on the basis of a subsonic analysis which removes the theoretical restriction for the attainment of intersonic crack tips speeds of the type that exist in homogeneous materials.

Despite these initial attempts, the phenomenon of intersonic crack propagation is still more or less unexplored. The experimental evidence is quite limited and still there does not exist a completely physically realistic theoretical model for the intersonically propagating interfacial crack. In view of these limitations, the current study presents valuable experimental observations on interface failure in the intersonic regime and interprets these observations based on currently available theory.

## EXPERIMENTAL TECHNIQUES

The two techniques of coherent gradient sensing (CGS) and photoelasticity were employed independently to study intersonic crack propagation along a bimaterial interface subjected to impact loading. Both these optical techniques provide real-time full field information and are ideally suited to investigate dynamic fracture events when used in conjunction with high-speed photography. However, the two techniques have their own advantages and limitations and the information provided is complementary. Hence, employing both the techniques allows for a better understanding of the dynamic fracture process. This will become apparent when the two techniques are discussed in the following sections.

### *Coherent Gradient Sensing interferometer (CGS)*

Figure 1 shows a schematic of the CGS setup in a transmission configuration. A coherent, monochromatic, collimated laser beam is incident on the bimaterial specimen. After transmission through the transparent side of the deforming specimen, it acquires an optical path difference and loses collimation. The optical path difference acquired is due to stress induced differences in refractive index and due to a non-uniform contraction in the thickness direction around the vicinity of the crack tip (Poisson's ratio effect for elastic solids). The resulting, non-collimated, beam passes through two line diffraction gratings  $G_1$  and  $G_2$  of fine pitch  $p$  (typically 40 lines/mm).

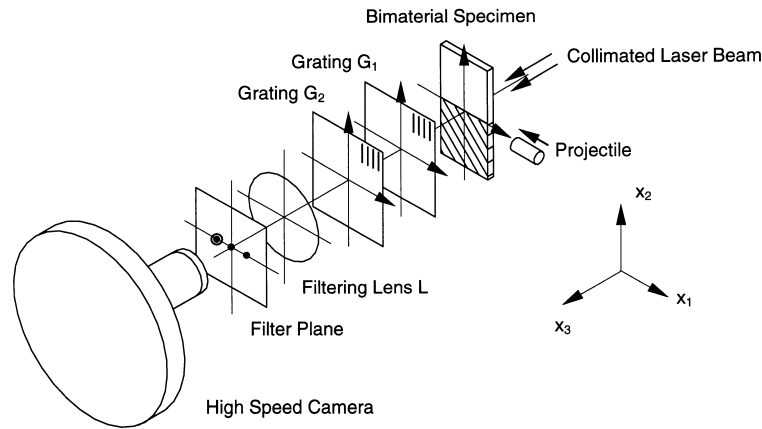


Fig. 1. Schematic of CGS setup in transmission. PMMA/steel bimaterial specimen is illustrated.

The gratings are situated a distance  $\Delta$  (typically 30–50 mm) apart and perform a “shearing” of the incident wave front. The gratings’ output intensity is transmitted through a filtering lens L. A diffraction spot pattern is obtained on the filtering plane, which is located at the back focal plane of lens L. On this plane all but one diffraction orders are blocked. The one remaining diffraction spot (either of  $\pm 1$  orders), shown in Fig. 1 as the open circle on the filtering plane, is imaged to produce an interference pattern. For the case of a dynamic experiment the imaging device is a high-speed camera focused on the specimen.

The details of analyzing the CGS optical method can be found in several previous articles including Tippur *et al.* (1991) and Rosakis (1993) and will not be repeated here for the sake of brevity. The condition for formation of constructive CGS interference fringes on the image plane, for gratings with lines parallel to the  $x_2$ -direction, is,

$$\frac{\partial(S(x_1, x_2))}{\partial x_1} = \frac{mp}{\Delta}, \quad m = 0, \pm 1, \pm 2, \dots \quad (1)$$

Where,  $S(x_1, x_2)$  is the optical path change that is introduced due to specimen deformation at a certain location in the  $x_1$ - $x_2$  plane. It has also been assumed that the diffraction gratings  $G_1$  and  $G_2$  are close enough and/or fine enough to obtain an interferogram that represents the  $x_1$ -gradient of  $S$ , rather than an  $x_1$ -finite difference of  $S$ . If the grating lines are parallel to the  $x_1$  direction then it can be shown that the condition for constructive interference becomes

$$\frac{\partial(S(x_1, x_2))}{\partial x_2} = \frac{np}{\Delta}, \quad n = 0, \pm 1, \pm 2, \dots \quad (2)$$

For the case of plane stress and a transmission configuration the quantity  $S(x_1, x_2)$  is related to the stress state in the deforming specimen as (Rosakis, 1993),

$$S(x_1, x_2) \approx c_\sigma h [\sigma_{11}(x_1, x_2) + \sigma_{22}(x_1, x_2)]. \quad (3)$$

Where  $c_\sigma$  is a stress optical coefficient for the material,  $h$  is the specimen thickness and  $\hat{\sigma}_{11}$  and  $\hat{\sigma}_{22}$  are thickness averages of the in-plane stress components in the plate.

For points outside the near tip three-dimensional region the CGS patterns assume a simple interpretation in terms of two-dimensional stress field approximations. In particular, eqns (1) and (2) in conjunction with eqn (3) now indicate that the fringes obtained from regions surrounding the three-dimensional zone can be related to the in-plane gradients of  $\hat{\sigma}_{11} + \hat{\sigma}_{22}$  as follows,

$$c_\sigma h \frac{\partial(\hat{\sigma}_{11} + \hat{\sigma}_{22})}{\partial x_1} = \frac{mp}{\Delta}, \quad c_\sigma h \frac{\partial(\hat{\sigma}_{11} + \hat{\sigma}_{22})}{\partial x_2} = \frac{np}{\Delta}, \quad m, n = 0, \pm 1, \pm 2, \dots \quad (4)$$

Where, in the case of transmission,  $c_\sigma$  is the stress optical coefficient of the transparent material.

The CGS interferograms are imaged by a rotating mirror type high-speed camera (Cordin Co., model 330A). The camera records 80 frames of the dynamic event and is typically operated at an interframe time of  $1.2 \mu\text{s}$  (about 840,000 frames/s). Individual frames are obtained by operating the laser light source (Spectra-Physics Argon-ion laser, model 166-09; operating wavelength  $\lambda = 514.5 \text{ nm}$  light) in a pulsed mode. The exposure time used in all experiments (i.e., the laser pulse duration) is 30 ns and the image is recorded on 35-mm black and white film (Kodak TMAX-3200).

Note that in this case the CGS interferograms represent contours of constant gradients of the first stress invariant,  $\hat{\sigma}_{11} + \hat{\sigma}_{22}$ , of the thickness averaged stress tensor in plane stress,  $\hat{\sigma}$ . This invariant can also be expressed in terms of the principal stresses of  $\hat{\sigma}$  as follows:  $\hat{\sigma}_{11} + \hat{\sigma}_{22} = \hat{\sigma}_1 + \hat{\sigma}_2$ , since  $\hat{\sigma}_{33} = \hat{\sigma}_3 = 0$ . Thus, the technique of CGS will not be sensitive to changes in the individual components of stress as long as the derivative of  $\hat{\sigma}_1 + \hat{\sigma}_2$  remains a constant.

### Photoelasticity

A schematic of the photoelastic setup in a transmission configuration is shown in Fig. 2. The specimen is placed in the optical bench of a high speed Cranz-Schardin spark-gap camera. The optical setup consists of two field lenses,  $F_1$  and  $F_2$ , and two circular polarizers,  $C_1$  and  $C_2$ . The first field lens,  $F_1$ , collimates white light from the

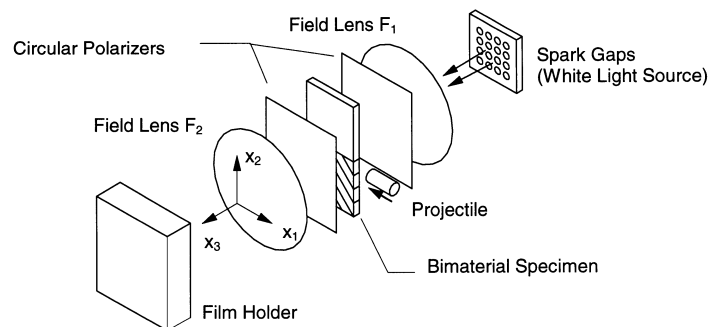


Fig. 2. Schematic of photoelasticity setup in transmission. Homalite-100/aluminum bimaterial specimen is illustrated.

spark-gaps that is incident on the specimen, while the second field lens,  $F_2$ , focuses the light transmitted through the specimen onto the film plane of the high speed camera. Meanwhile, the two circular polarizers form a circular polariscope, which allow photoelasticity to be used to observe the state of stress in the specimen. The transparent side of the bimaterial specimen is specially chosen so that it exhibits stress induced birefringence, which is a fundamental requirement of this technique. A filter (Kodak Wratten filter no. 8) is placed before the film plane of the high speed camera, so that only fringes corresponding to a particular wavelength of light are recorded. The technique of photoelasticity is very well established for a variety of solid mechanics applications and the reader is referred to Dally and Riley (1991) for further details.

The generation of isochromatic fringe patterns is governed by the stress optic law. For the case of monochromatic light, the condition for the formation of fringes is expressed as,

$$\hat{\sigma}_1 - \hat{\sigma}_2 = \frac{Nf_\sigma}{h}, \quad (5)$$

where,  $\hat{\sigma}_1 - \hat{\sigma}_2$  is the principal stress difference of the thickness averaged stress tensor,  $\hat{\sigma}$ ,  $f_\sigma$  is the material fringe value,  $h$  is the specimen thickness and  $N$  is the isochromatic fringe order. The isochromatic fringe patterns observed are contours of constant maximum shear stress,  $\hat{\tau}_{\max} = (\hat{\sigma}_1 - \hat{\sigma}_2)/2$ .

The photoelastic fringe patterns are imaged using a high speed Cranz-Schardin spark-gap camera. The camera provides a total of twenty images of the dynamic fracture event at an interframe time of  $4 \mu\text{s}$  (250,000 frame/s). The spark-gaps serve as the light sources and the exposure time is typically 400 ns, as determined by the time duration of the sparks. The recording medium is once again black and white photographic film (Kodak Professional  $8' \times 10'$  film no. 4127).

#### *Bimaterial specimen and loading arrangement*

The bimaterial specimens used in these experiments consisted of a transparent polymer bonded directly to a metal. The material combinations were chosen so that there would be a large mismatch in the mechanical properties across the interface and this would intensify the dynamic effects. The particular choice of the transparent polymer was also dictated by the particular needs of the experimental technique employed, i.e. CGS or photoelasticity. For the case of CGS, the transparent half was Plexiglas (Polymethylmethacrylate or PMMA) while the metal half was AISI 4340 steel. For the photoelastic experiments, the transparent half was Homalite-100, a polyester resin that exhibits stress induced birefringence, while the metal half was 6061 aluminum. Throughout this paper, the transparent polymer side of the specimen will be referred to as material-1 and the metal side as material-2.

Mechanical properties of the material constituents are listed in Table 1. Since both PMMA and Homalite-100 exhibit rate sensitivity their properties are listed for two extreme strain rates [ $\dot{\epsilon} = 10^{-3} \text{ s}^{-1}$  and  $\dot{\epsilon} = 10^3 \text{ s}^{-1}$  (glassy state)] that could be encountered by material elements in the vicinity of the propagating crack tip. In reality the material surrounding the propagating crack tip is not subject to any uniform value of strain rate. Instead there is a strain rate distribution around the crack tip, which

Table 1. *Mechanical properties and wave speeds of interface constituents*

Property	PMMA		Homalite-100 <sup>1</sup>		4340 Steel	6061 Aluminum
	$\dot{\epsilon} = 10^{-3} \text{ s}^{-1}$	$\dot{\epsilon} = 10^3 \text{ s}^{-1}$	$\dot{\epsilon} = 10^{-3} \text{ s}^{-1}$	$\dot{\epsilon} = 10^3 \text{ s}^{-1}$		
Young's modulus, $E$ (GPa)	3.2	5.6	3.9	5.3	208	71
Poisson's ratio, $\nu$	0.35	0.35	0.35	0.35	0.3	0.33
Density, $\rho$ (kg/m <sup>3</sup> )	1190	1190	1230	1230	7830	2770
Dilatational wave speed, $c_l$ (m/s)	1760	2330	1890	2220	5400	5430
(plane-stress)						
Shear wave speed, $c_s$ (m/s)	1000	1330	1080	1270	3195	3100
Rayleigh wave speed, $c_R$ (m/s)	935	1243	1010	1185	2950	2890
Material fringe value, $f_o$ (kN/m)	—	—	—	23.7	—	—
$\epsilon^{\text{PMMA/steel}} = 0.1037$ $\epsilon^{\text{PMMA/rigid}} = 0.1073$ $\epsilon^{\text{Homalite-100/aluminum}} = 0.0912$ $\epsilon^{\text{Homalite-100/rigid}} = 0.1073$						

<sup>1</sup>Manufactured by Homalite Inc., Delaware, U.S.A.

depends on the crack tip stress field. Thus, the material wave speeds at any given point of observation would depend on the effective strain rate at that point and would lie between the two extreme values listed in Table 1. It should be noted that neither 6061 aluminum nor 4340 steel exhibit any appreciable strain rate sensitivity for the strain rates in consideration.

As shown in Table 1, either of the PMMA/steel or the Homalite-100/aluminum combination results in a significant mismatch of mechanical properties and, most importantly for dynamics, wave speeds across the bimaterial interface. The values of the plane-stress quasi-static oscillatory index  $\varepsilon$  are also listed for PMMA/steel, PMMA/rigid, Homalite-100/aluminum and Homalite-100/rigid material combinations. As demonstrated by these values, both the material combinations behave very similar to an elastic/rigid bimaterial system. Thus, one can expect intensified interfacial effects during the dynamic fracture event.

The specimen preparation procedure for both the material combinations is the same in principle. The bonding is achieved using the monomer of the transparent polymer in conjunction with appropriate catalysts/hardening-agents. Bonding for the PMMA/steel interface is described by Tippur and Rosakis (1991) while that for the Homalite-100/aluminum interface by Singh and Shukla (1996). The issue of bond strength and toughness has also been addressed by the same authors.

The bimaterial specimens were subjected to one-point bend type impact loading as shown in Fig. 3. The impact was achieved by using a cylindrical steel projectile launched using a pressurized gas-gun. For the CGS experiments the projectile was 75 mm long and 50 mm in diameter, and the impact velocity was 20 m/s. Meanwhile, for the photoelastic experiments the projectile was 100 mm long and 12.5 mm in diameter, and the impact velocity was 30 m/s. As will be shown later, both these loadings result in essentially the same mode of bimaterial failure. It is apparent that the loading history experienced by the crack tip would depend on whether the specimen was impacted on the polymer side or the metal side of the interface. In all these experiments the specimen was impacted from the metal side of the interface, so that the energy to the propagating crack tip would be supplied from the side with the higher stress-wave speeds.

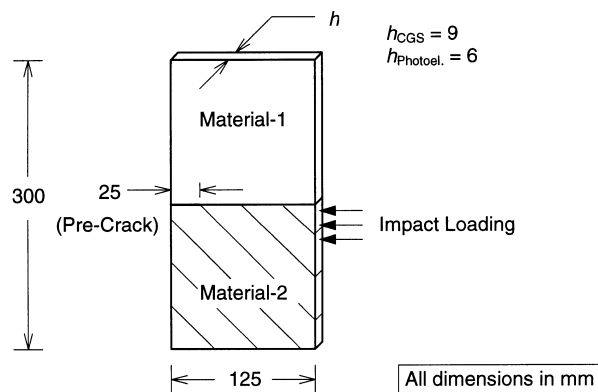


Fig. 3. Bimaterial specimen showing the one point bend impact geometry.

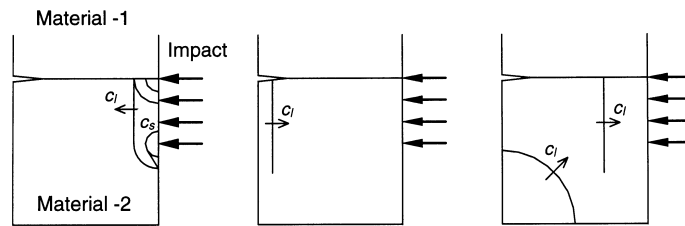


Fig. 4. Stress wave loading of the interfacial crack tip arising from the one point bend impact, (a) just after impact, (b) just before initiation and (c) during crack growth.

The nature of the loading arrangement results in the interface crack tip being loaded primarily in shear. The projectile impacting the metal side of the specimen generates stress wave fronts as shown in Fig. 4(a). The main compressive dilatational stress wave traverses the width of the metal specimen. When this wave passes by the pre-crack tip at the interface it loads the crack tip primarily in shear. This compressive dilatational stress wave then reflects from the opposite free surface as a tensile wave and again propagates by the crack-tip on the interface going in the opposite direction. Doing so it enhances the state of shear that exists around the crack tip (doubles the particle velocity in the negative  $x_1$ -direction), resulting in crack initiation and crack extension. The acoustic mismatch across the bimaterial interface greatly impedes the transfer of stress waves from the metal to the polymer. Hence, the interface crack is driven from the metal side and primarily in a state of shear. Note that at later times other reflections from the specimen boundaries will also impinge upon the interface, as shown in Fig. 4(c), and will change the nature of loading. However, these effects occur later on in the time history of the fracture process.

## RESULTS AND DISCUSSION

### *Observation of contact and shear mach wave*

A typical selected sequence of CGS interferograms from a one point bend experiment on a PMMA/steel specimen is shown in Fig. 5 (Lambros and Rosakis, 1995a). Note that the CGS fringes are observed only in the transparent side (i.e. the PMMA side) of the specimen. The instantaneous location of the crack tip is known from each frame and this was used to determine the history of the crack tip speed. A typical crack tip speed history obtained from one such experiment is plotted in Fig. 6. The shear wave speed of PMMA,  $c_s^{\text{PMMA}}$ , is also plotted in the same figure for two extreme loading rates [ $\dot{\epsilon} = 10^{-3} \text{ s}^{-1}$  and  $\dot{\epsilon} = 10^3 \text{ s}^{-1}$  (glassy state)] that may be typically expected in the region surrounding the propagating crack tip. The effective shear wave speed at a given point of observation would depend on the effective strain rate at that point and thus would lie between the two extreme values shown in Fig. 6. After initiation the crack tip accelerated very rapidly to beyond the upper extreme of the shear wave speed of PMMA. Then the crack tip speed oscillated between the upper and lower extremes of  $c_s^{\text{PMMA}}$  for about  $15 \mu\text{s}$ , after which it accelerated even

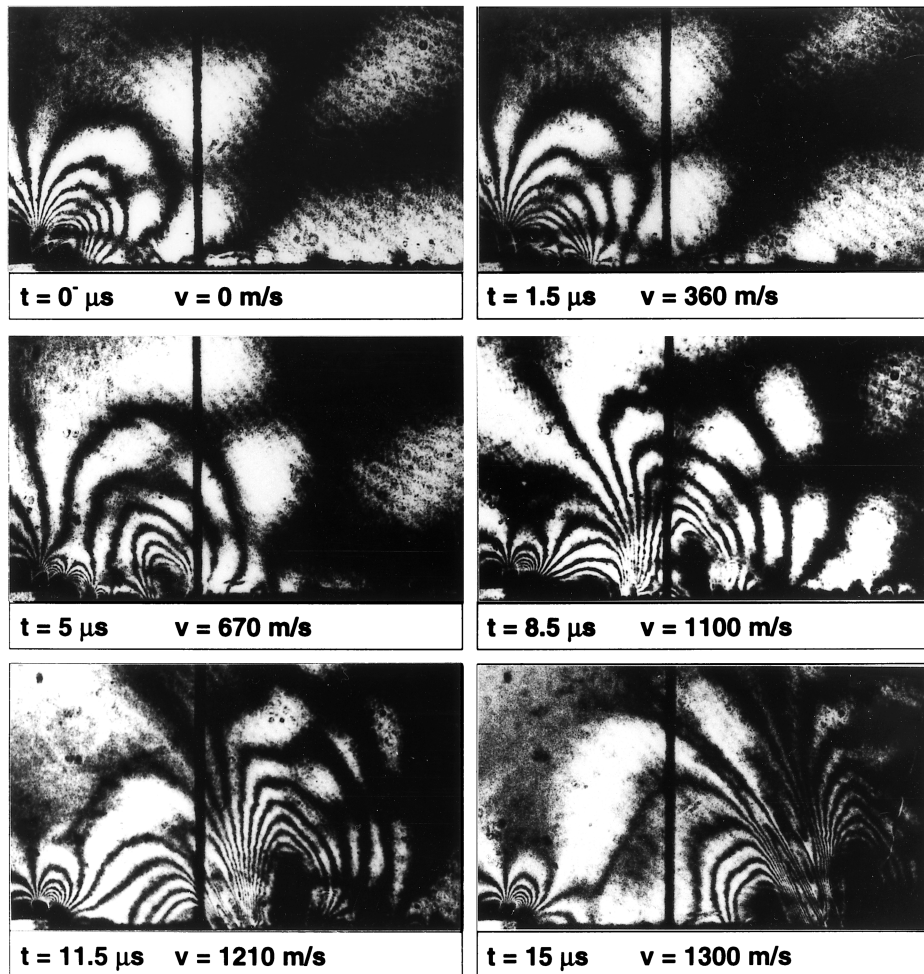


Fig. 5. Typical set of CGS interferograms obtained for dynamic crack growth along a PMMA/steel bimaterial interface subjected to impact loading.

further. Crack tip accelerations were of the order of  $10^8$  m/s<sup>2</sup>, which establishes the highly unstable nature of this crack tip event. This dynamic and highly repeatable variation of the crack tip speed was first observed by Lambros and Rosakis (1995a) and explained by Lambros and Rosakis (1995c) and Liu *et al.* (1995).

Tests conducted with Homalite-100/aluminum specimens, using the technique of photoelasticity, yield similar observations despite the fact that now different materials constitute the bimaterial interface. Figure 7 shows a typical set of isochromatic fringe patterns obtained for dynamic crack propagation along a Homalite-100/aluminum bimaterial surface (Singh and Shukla, 1996). The history of the crack tip speed typically observed for these experiments is plotted in Fig. 8. As observed for the PMMA/steel case the crack tip accelerated very rapidly after initiation to beyond the

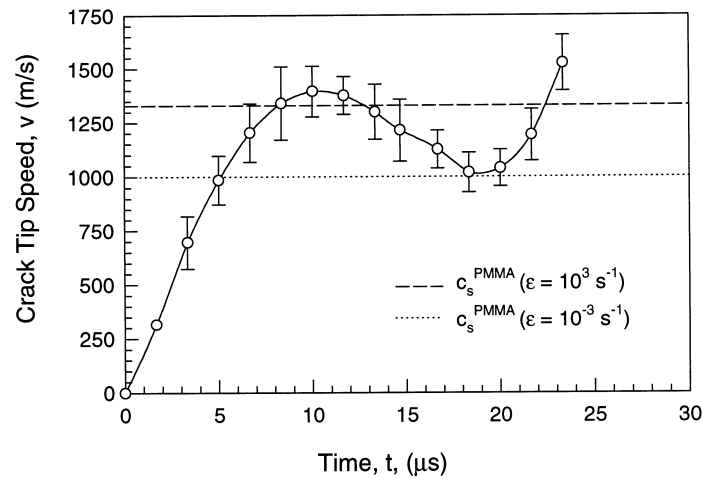


Fig. 6. Typical crack tip speed history for dynamic crack growth along a PMMA/steel bimaterial interface subjected to impact loading.

upper extreme of the shear wave speed of material-1 (Homalite-10). Thereafter, the crack tip speed stayed at this value for about 20  $\mu\text{s}$ , after which it accelerated even further.

The terminal crack tip speeds that have been observed for these experiments were about 140% of the upper extreme of  $c_s^{\text{PMMA}}$  for the PMMA/steel bimaterial interface and about 130% of the upper extreme of  $c_s^{\text{Homalite-100}}$  for the Homalite-100/aluminum bimaterial interface. Nevertheless, the dilatational wave speed of material-1 (PMMA or Homalite-100) was not exceeded in either case. Crack growth in this speed regime is termed as being intersonic.

Crack propagation in the intersonic regime has a direct effect on the nature of the fringe patterns observed. At first the fringes are smooth and continuous, while the crack tip is still subsonic, as shown in the first few frames in Figs 5 and 7. Moreover, the forward and rear fringe loops focus at a single point along the interface, which is the crack tip. In subsequent frames, however, the fringes become squeezed and elongated normal to the interface. Finally, in the intersonic crack growth regime, the fringes in the center of the two lobed fringe pattern do not seem to focus to a single point along the interface. Instead they intercept the bond line over a finite area between the two main lobes, which is evident in the last frame in Fig. 5 and the last three frames in Fig. 7. This effect is seen clearly in Fig. 9, in which the length of the area between the front and back lobes is identified as  $l$ . The fringe pattern in this particular frame is caused by large scale contact of the crack faces along  $l$ , as the crack is propagating in the intersonic regime. This large-scale contact of crack faces was first observed by Lambros and Rosakis (1995c), theoretically confirmed by Liu *et al.* (1995), and also observed by Singh and Shukla (1996). From the numerical simulation point of view, Xu and Needleman (1996) have confirmed the existence of a contact zone area when the crack tip speed exceeds the lower of the two Rayleigh wave speeds.

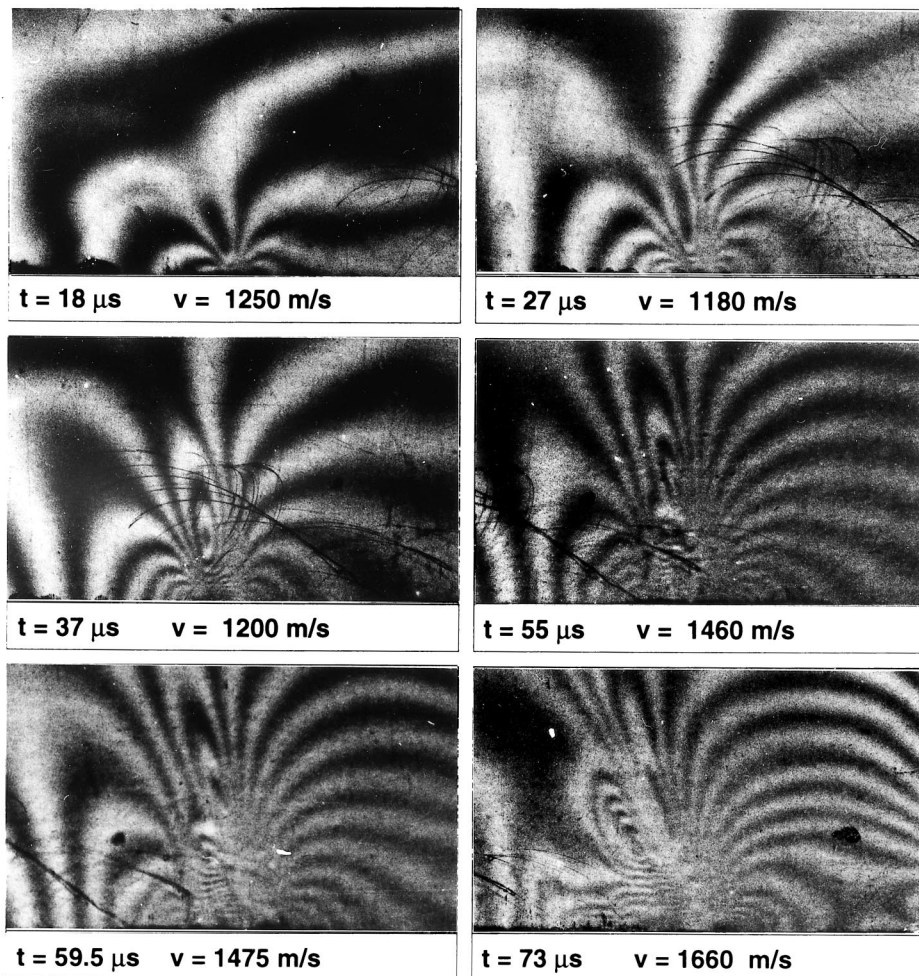


Fig. 7. Typical set of isochromatic fringe patterns obtained for dynamic crack growth along a Homalite-100/aluminum bimaterial interface subjected to impact loading.

Another direct consequence of intersonic crack propagation is the formation of a mach wave (or line-of-discontinuity) in the stress field surrounding the moving crack tip. The propagating crack tip acts as a source of shear and dilatational stress waves, which radiate out into the material and establish the stress field that surrounds the crack tip. If this source (the crack tip) propagates faster than the shear wave speed then the spreading out of the shear waves is limited and a mach wave (or line-of-discontinuity) forms. The existence of such mach waves was predicted by the analysis of Liu *et al.* (1995) but could not be confirmed by the earlier CGS experiments. Note that by the very nature of the technique, CGS would not be sensitive to these discontinuities in the stresses and hence the mach wave would not show up in the

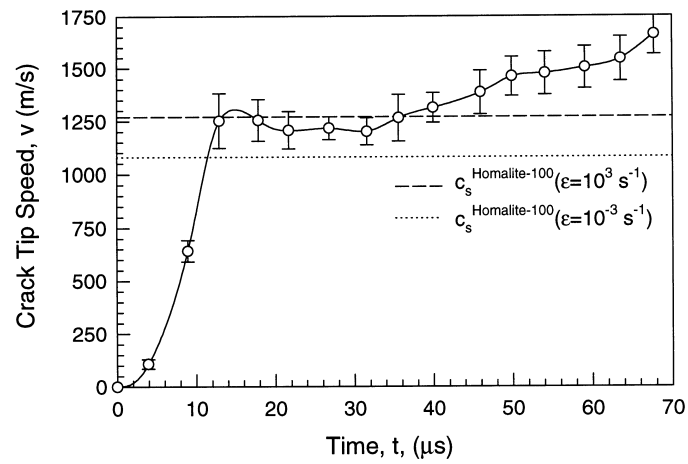


Fig. 8. Typical crack tip speed history for dynamic crack growth along a Homalite-100/aluminum bimaterial surface interface subjected to impact loading.

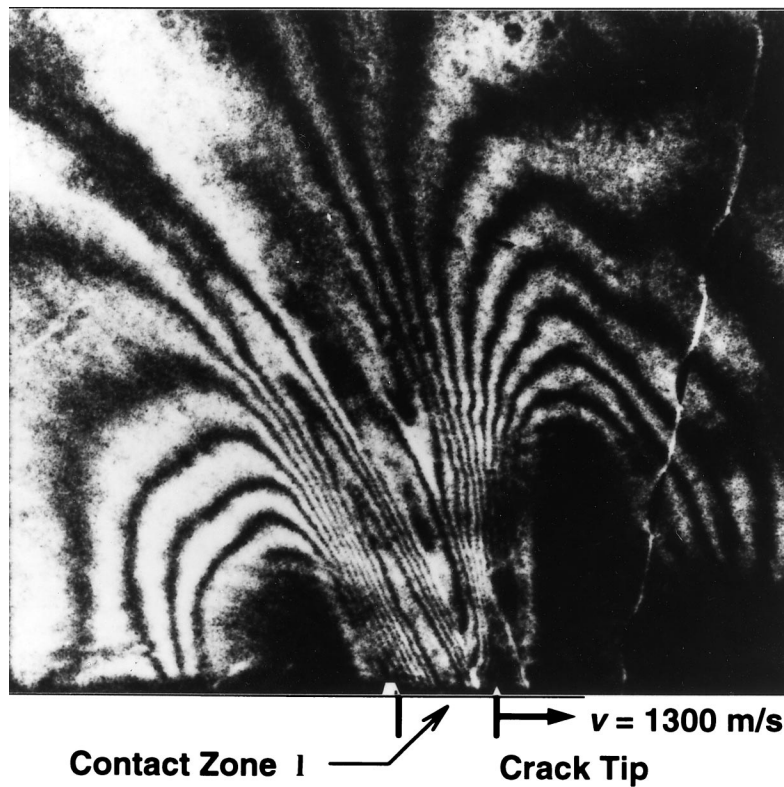


Fig. 9. Enlarged view of CGS fringes in the intersonic crack growth regime showing the area of crack face contact.

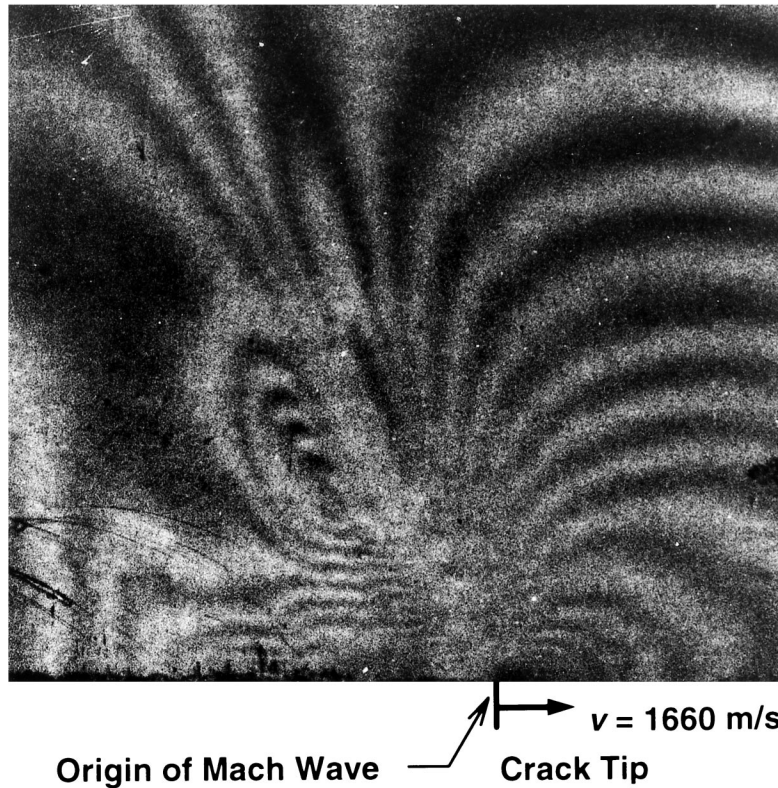


Fig. 10. Discontinuities of isochromatic fringe contours representing the formation of a mach wave.

CGS interferograms. Experimental evidence of the mach wave is observed in the photoelasticity experiments in the form of discontinuous isochromatic fringe contours as shown in Fig. 10. The line originates at the crack tip and radiates out into the material. To the authors' knowledge this is the first direct observation of mach wave formation resulting from intersonic crack propagation along a bimaterial interface.

*Intersonic crack growth along an elastic/rigid interface*

It was noted earlier that both the PMMA/steel and Homalite-100/aluminum bimaterial systems can be modeled very well by an elastic/rigid approximation. Now, consider a crack propagating intersonically along an elastic/rigid interface, as shown in Fig. 11. Using an asymptotic analysis Liu *et al.* (1995) have shown that the stress field around the crack tip can be expressed as,

$$\sigma_{ij} = \frac{\mu A_0}{1 + \alpha_i^2 \alpha_s^2} \left\{ \frac{\Sigma_{ij}^a}{r^q} + \frac{\Sigma_{ij}^b}{(\eta_1 + \hat{\alpha}_s \eta_2)^q} H(\eta_1 + \hat{\alpha}_s \eta_2) + \frac{\Sigma_{ij}^c}{(-\eta_1 - \hat{\alpha}_s \eta_2)^q} H(-\eta_1 - \hat{\alpha}_s \eta_2) \right\}, \tag{6}$$

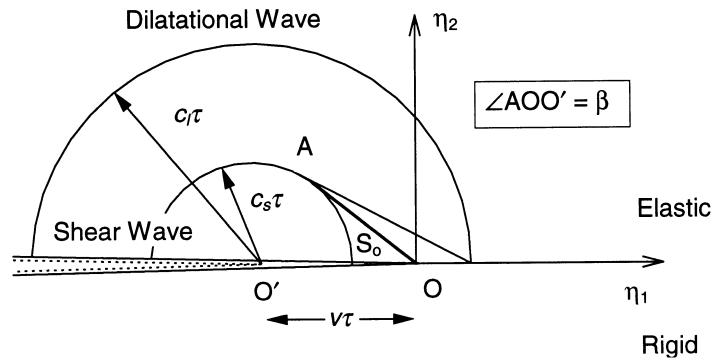


Fig. 11. A crack propagating intersonically along an elastic/rigid interface.

$$\alpha_l^2 = 1 - \frac{v^2}{c_l^2}, \quad \alpha_s^2 = \frac{v^2}{c_s^2} - 1. \tag{7}$$

Where,  $v$  is the crack tip speed ;  $\mu$ ,  $c_l$  and  $c_s$  are the shear modulus, dilatational wave speed and shear wave speed, respectively, of material-1 and  $H(\cdot)$  is the Heaviside unit step function. Also, the functions  $\Sigma_{ij}^a$ ,  $\Sigma_{ij}^b$  and  $\Sigma_{ij}^c$  are functions of  $\theta_i$ , the crack tip speed,  $v$ , and the wave speeds of material-1,  $c_l$  and  $c_s$ . The scaled polar coordinates are defined as,

$$r_i = \sqrt{\eta_1^2 + \alpha_l^2 \eta_2^2}, \quad \theta_i = \arctan \left( \frac{\alpha_l \eta_2}{\eta_1} \right). \tag{8}$$

Finally, the strength of the crack tip singularity is given as,

$$q(v) = \frac{1}{\pi} \arctan \left\{ \frac{\alpha_l \alpha_s [4 - (1 - \alpha_s^2)^2]}{4 \alpha_l^2 \alpha_s^2 + (1 - \alpha_s^2)^2} \right\}. \tag{9}$$

The variation of the singularity exponent,  $q(v)$ , with crack tip speed,  $v$ , is plotted in Fig. 12 for different values of the Poisson’s ratio of the elastic material. The exponent starts at a value of  $q(v) = 0$  at  $v = c_s$  and increases monotonically with crack tip speed till it reaches a maximum value at  $v = \sqrt{2}c_s$ . With further increase in the crack tip speed the exponent decreases monotonically back to the value  $q = 0$ . Note that  $q(v)$  remains less than 0.5 for the entire speed range considered. This limit on the maximum value of  $q(v)$  implies that energy flux into the moving crack tip is always zero irrespective of the crack tip speed in the intersonic crack growth regime.

The asymptotic analysis is very useful in explaining several key features of intersonic crack propagation along bimaterial interfaces. The first result is that across the head wave front  $S_0$ , see Fig. 11, the components of stress and particle velocity are discontinuous. Therefore, unlike subsonic crack growth where only one singular point is present at the crack tip, for the case of intersonic crack growth, an entire singular line of infinite jumps in stress and particle velocity appears in the body. The singularity across this line is the same as that at the crack tip. The line originates from the

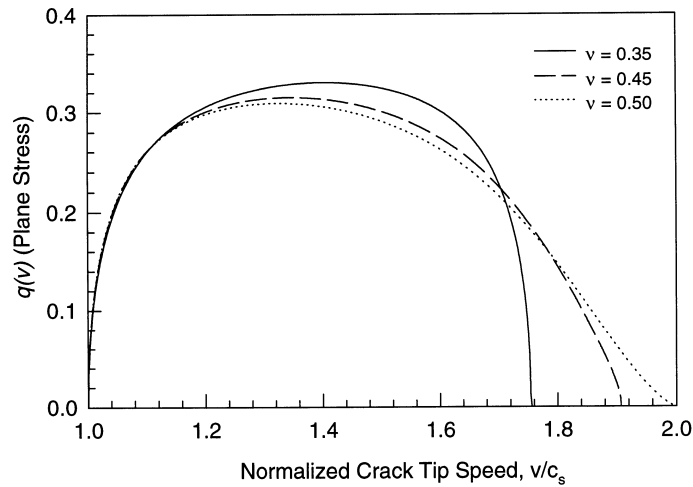


Fig. 12. Variation of the singular exponent  $q(v)$  as a function of crack tip speed  $v$  for different values of Poisson's ratio (Liu *et al.*, 1995).

propagating crack tip and radiates out into the elastic solid. The existence of such a discontinuity is evident by inspection of eqn (6) shown above. This is the line-of-discontinuity that appears in the isochromatic fringe patterns obtained in the photoelastic experiments. The equation of the moving line of discontinuity is given by,

$$\eta_1 + \hat{\alpha}_s \eta_2 = 0. \tag{10}$$

Thus, the angular orientation of this line, with respect to the interface, can be expressed in terms of the crack tip speed,  $v$ , and the shear wave speed of the elastic material (or material-1),  $c_s$ , as,

$$\tan \beta = \frac{1}{\sqrt{\frac{v^2}{c_s^2} - 1}}. \tag{11}$$

The orientations of the line-of-discontinuity determined from the experimental isochromatic fringe patterns were compared with the angles predicted by the above equation and are listed in Table 2. The correspondence between the experimentally observed and theoretically predicted angles is excellent and substantiates the fact that the experimentally observed line-of-discontinuity is indeed the theoretically predicted mach wave. Further evidence of the line-of-discontinuity is presented in the numerical simulations of Xu and Needleman (1996). Liu *et al.* (1995) also showed that there is no energy dissipation when the singular line  $S_0$  moves through the elastic material.

Consider the normal tractions along the interface at an arbitrary distance  $a$  ahead of the moving crack tip,  $\sigma_{22}(a, 0^+, t)$ , and the crack opening displacement at the distance  $a$  behind the moving crack tip,  $u_2(-a, 0^+, t)$ . Then it can be shown (Liu *et al.*, 1995) that if the crack tip speed is in the range  $c_s < v < \sqrt{2}c_s$ ,  $\sigma_{22}(a, 0^+, t)$  and

Table 2. Comparison of experimentally measured and theoretically predicted orientations of the line-of-discontinuity

Frame number	$v/c_s^{\text{Homalite-100}}$	$\beta_{\text{Theory}}$ ( $^{\circ}$ )	$\beta_{\text{Experiment}}$ ( $^{\circ}$ )
13	1.16	59.5	63
14	1.19	57.5	55
15	1.21	55.7	53
16	1.30	50.3	48

$u_2(-a, 0^+, t)$  have opposite signs. This implies that when the normal traction ahead of the crack tip is positive, crack face penetration into the rigid substrate is predicted. Now, positive normal tractions ahead of the crack tip are required to facilitate interface rupture and crack face penetration is physically impossible. Hence, in the crack tip speed range  $c_s < v < \sqrt{2}c_s$  the crack faces would come into contact behind the propagating crack tip. This accounts for the large-scale contact of crack faces observed experimentally in the CGS interferograms when the crack tip speed was indeed in the range  $c_s^{\text{PMMA}} < v < \sqrt{2}c_s^{\text{PMMA}}$ . When the crack tip speed is in the range  $\sqrt{2}c_s < v < c_l$ , a positive normal traction ahead of the crack tip results in crack face opening behind the moving crack tip and no contact of the crack faces should be observed asymptotically. However, up to date, no observations of crack tip speeds greater than  $\sqrt{2}c_s$  have been made.

It should be noted at this point that in the intersonic regime the asymptotic crack tip field does not have the oscillatory nature characteristic of all subsonic crack growth solutions. In the subsonic cases it is this oscillatory nature that accounts for contact and interpenetration. As discussed by Rice (1988), in most cases, this ‘‘small scale’’ contact is of the order of  $10^{-8}L$ , where  $L$  is a characteristic length of the problem. The situation here is very different. The observed and predicted contact zones are large scale ( $l \approx 1\text{--}5$  mm) and are not a result of an oscillatory nature of the field. In the present scenario contact is related to the intersonic motion of the crack tip disturbance. Indeed this phenomenon is reminiscent of the intersonic motion of a line load on an elastic half-space. In this problem when the speed of the moving load exceeds the Rayleigh wave speed of the half-space the direction of surface displacements, under the load, is in opposition to the direction of loading as discussed by Georgiadis and Barber (1993).

When crack face contact does indeed occur, the asymptotic solution is no longer valid and the problem must be revisited under different crack face boundary conditions. Nevertheless, despite this limitation the solution does provide considerable conceptual insight into the intersonic crack growth phenomenon.

Some qualitative observations as above have been made for a more realistic elastic/elastic analysis for intersonic bimaterial crack growth (Huang *et al.*, 1996). Here again traveling mach waves have been predicted. Also, for certain crack tip speed range large-scale contact was implied by the solution. However, the details of the



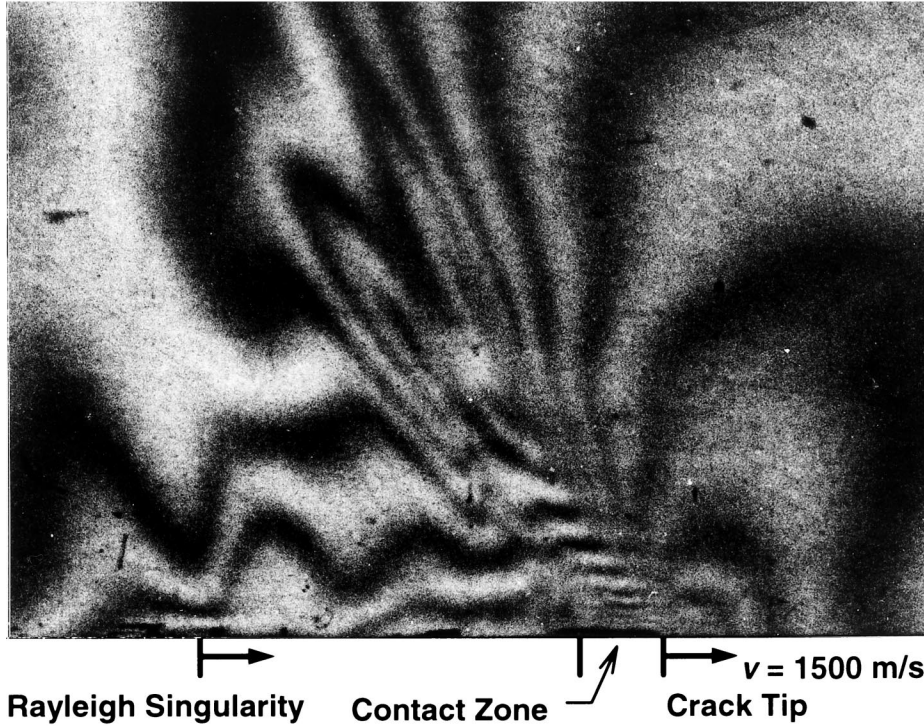


Fig. 14. Details of the isochromatic fringe patterns around the intersonically propagating crack tip showing the primary and secondary mach waves as lines-of-discontinuity, the dynamically moving contact zone, and the Rayleigh disturbance.

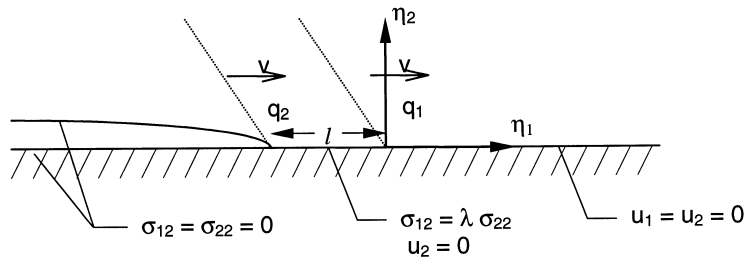


Fig. 15. An interface crack propagating intersonically between an elastic solid and a rigid substrate, with a finite contact zone of length  $l$  trailing the crack tip.

$$\begin{aligned}
 & - \frac{2\alpha_s \hat{\alpha}_s}{|R_1|^{q_1} |R_2|^{q_2}} \{ H(R_1) + (\cos q_1 \pi - \alpha_s \hat{\alpha}_s \sin q_1 \pi) [H(R_2) - H(R_1)] \} \\
 & + \frac{\hat{\alpha}_s^2 - 1}{|R_1|^{q_1} |R_2|^{q_2}} [(\alpha_s \hat{\alpha}_s \cos(q_1 + q_2)\pi + \sin(q_1 + q_2)\pi) H(-R_2)] \} \quad (12b)
 \end{aligned}$$

$$\begin{aligned} \sigma_{12} = & \frac{-\mu A_0}{1 + \alpha_l^2 \hat{\alpha}_s^2} \left\{ \frac{2\alpha_l}{r_1^{q_1} r_2^{q_2}} (\cos \beta - \alpha_l \hat{\alpha}_s \sin \beta) \right. \\ & - \frac{\alpha_l(1 - \hat{\alpha}_s^2)}{|R_1|^{q_1} |R_2|^{q_2}} \{H(R_1) + (\cos q_1 \pi - \alpha_l \hat{\alpha}_s \sin q_1 \pi)[H(R_2) - H(R_1)]\} \\ & \left. + \frac{(\hat{\alpha}_s^2 - 1)^2}{2\hat{\alpha}_s |R_1|^{q_1} |R_2|^{q_2}} [(\alpha_l \hat{\alpha}_s \cos(q_1 + q_2)\pi + \sin(q_1 + q_2)\pi)H(-R_2)] \right\}. \end{aligned} \quad (12c)$$

Where,  $\lambda$  is the friction coefficient,  $l$  is the contact length,  $H(x)$  is the Heaviside function, and

$$\eta_1 = x - vt \quad \eta_2 = y \quad (13)$$

$$\begin{aligned} r_1 &= \sqrt{\eta_1^2 + \alpha_l^2 \eta_2^2}, \quad \theta_1 = \arctan \left( \frac{\alpha_l \eta_2}{\eta_1} \right) \\ r_2 &= \sqrt{(\eta_1 + l)^2 + \alpha_l^2 \eta_2^2}, \quad \theta_2 = \arctan \left( \frac{\alpha_l \eta_2}{\eta_1 + l} \right) \end{aligned} \quad (14)$$

$$\alpha_l = \sqrt{1 - \frac{v^2}{c_l^2}}, \quad \hat{\alpha}_s = \sqrt{\frac{v^2}{c_s^2} - 1} \quad (15)$$

$$R_1 = \eta_1 + \hat{\alpha}_s \eta_2, \quad R_2 = \eta_1 + \hat{\alpha}_s \eta_2 + l \quad (16)$$

$$\begin{aligned} q_1 &= \frac{1}{\pi} \tan^{-1} \left[ \frac{\alpha_l(1 + \hat{\alpha}_s^2)(1 + \lambda \hat{\alpha}_s)}{\alpha_l^2 \hat{\alpha}_s(1 + \hat{\alpha}_s^2 + 2\lambda \hat{\alpha}_s) + \lambda(1 - \hat{\alpha}_s^2)} \right] \\ q_2 &= \frac{1}{\pi} \tan^{-1} \left[ \frac{\alpha_l(1 - \hat{\alpha}_s^4)[2\lambda \hat{\alpha}_s - (1 - \hat{\alpha}_s^2)]}{4\alpha_l^2 \hat{\alpha}_s(1 + \hat{\alpha}_s^2 + 2\lambda \hat{\alpha}_s) + \lambda(1 - \hat{\alpha}_s^2)^3} \right] \end{aligned} \quad (17)$$

$$\beta = q_1 \theta_1 + q_2 \theta_2. \quad (18)$$

The functions  $q_1$  and  $q_2$  represent the singularity strengths at the crack tip and at the end of the contact zone. For a far-field observer located at  $r = L \gg l$  the crack tip and the end of the contact zone appear as one and have a stress singularity given as

$$q = q_1 + q_2. \quad (19)$$

Where, the coefficient  $q$  is the same as defined by eqn (9) and plotted in Fig. 12.

The solution features a large-scale contact zone and predicts two distinct traveling mach waves, one emanating from the crack tip and the other from the end of the contact zone. Moreover, it also predicts a non-zero energy dissipation rate due to frictional dissipation associated with the contact region. Figure 16 shows representative isochromatic fringe patterns generated using the crack tip stress fields given in eqn (12). Here the crack tip is propagating with velocity  $v = 1.2c_s$  as for the experimental case shown in Fig. 14. The theoretically generated fringe patterns show

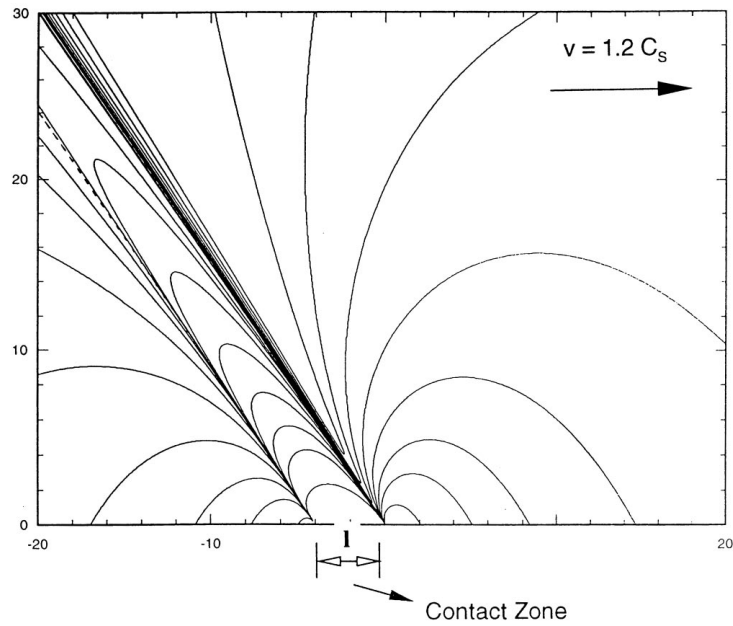


Fig. 16. Representative isochromatic fringe patterns generated using the asymptotic crack-tip stress fields (Yang *et al.*, 1997).

the existence of two distinct mach waves, one emanating from the crack tip and the other from the trailing edge of the contact zone.

#### *Future directions*

Motivated by the critical crack opening and shearing displacement criterion for subsonic crack growth along a bimaterial interface (Lambros and Rosakis, 1995b) a fracture growth criterion has also been proposed for the case of intersonic crack growth along a bimaterial interface (Huang *et al.*, 1997). In the absence of opening displacements in the contact zone for intersonically growing interface cracks (as depicted in Fig. 15) it is postulated that intersonic crack growth will take place in the presence of a critical sliding displacement evaluated at the end of the contact zone (Huang *et al.*, 1997),

$$u_1(\eta_1 = -l, \eta_2 = 0^+) = \delta_c. \quad (20)$$

Where,  $\delta_c$  is the critical value of the sliding displacement and depends only on bimaterial and bond properties. Based upon eqn (20) it is possible to express the normalized energy dissipation rate associated with the propagating crack as a function of the crack tip speed. Figure 17 shows the variation of the normalized energy dissipation rate as a function of crack tip speed for the case of a positive coefficient of contact friction,  $\lambda$ . For this specific case it is found that the energy dissipation rate has a large but finite value at  $c_s$ . This suggests that there exists a finite energy barrier

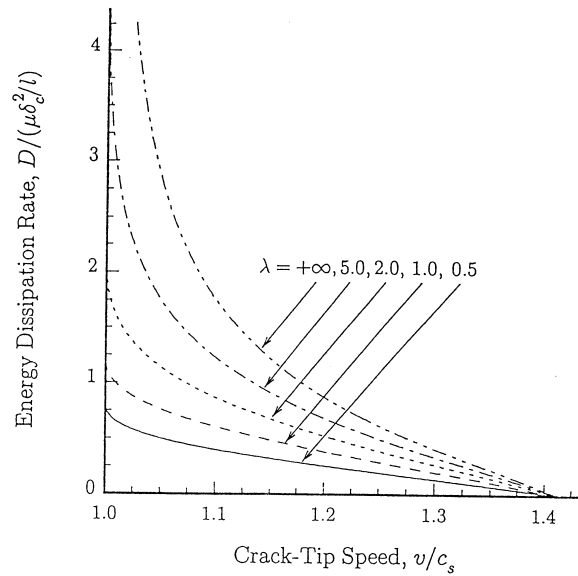


Fig. 17. Normalized energy dissipation rate for intersonic crack propagation along an elastic/rigid interface (Yang *et al.*, 1997).

at the velocity  $c_s$ , which is consistent with experimental observations (Liu *et al.*, 1993; Lambros and Rosakis, 1995c; Singh *et al.*, 1997). In these experiments it was observed that the crack seemed to favor growth at  $v = c_s$  and stayed at this speed for a substantial period of time before accelerating further in an unstable fashion. Indeed, the unstable acceleration of the crack tip beyond  $\sqrt{2}c_s$  is consistent with the decreasing energy dissipation rate, as shown in Fig. 17.

Very recent experiments conducted on the PMMA/Aluminum bimaterial system have demonstrated that it is possible for bimaterial cracks to propagate at speeds even greater than  $\sqrt{2}c_s$  of the more compliant material (i.e. PMMA). These experiments employed the same specimen geometry and loading arrangement as before. However, the time window of observation was extended to observe more of the fracture process. A typical selected sequence of CGS interferograms from such an experiment is shown in Fig. 18. Note that, as before, the CGS fringes are observed only in the PMMA side of the specimen. The history of the crack tip speed obtained from this experiment is plotted in Fig. 19. It can be seen that the crack propagates for some time in the regime  $c_s^{\text{PMMA}} < v < \sqrt{2}c_s^{\text{PMMA}}$  before accelerating further in a rapid unstable fashion. Terminal crack tip speeds in this case have exceeded not only the plane wave speed of PMMA,  $c_t^{\text{PMMA}}$ , but also the Rayleigh wave speed of aluminum. Thus, this is the case of crack growth being truly supersonic with respect to the compliant half of the bimaterial interface. Note that once  $\sqrt{2}c_s^{\text{PMMA}}$  has been exceeded there is no further requirement for crack face contact and the model depicted in Fig. 15 must be revisited and suitably modified.

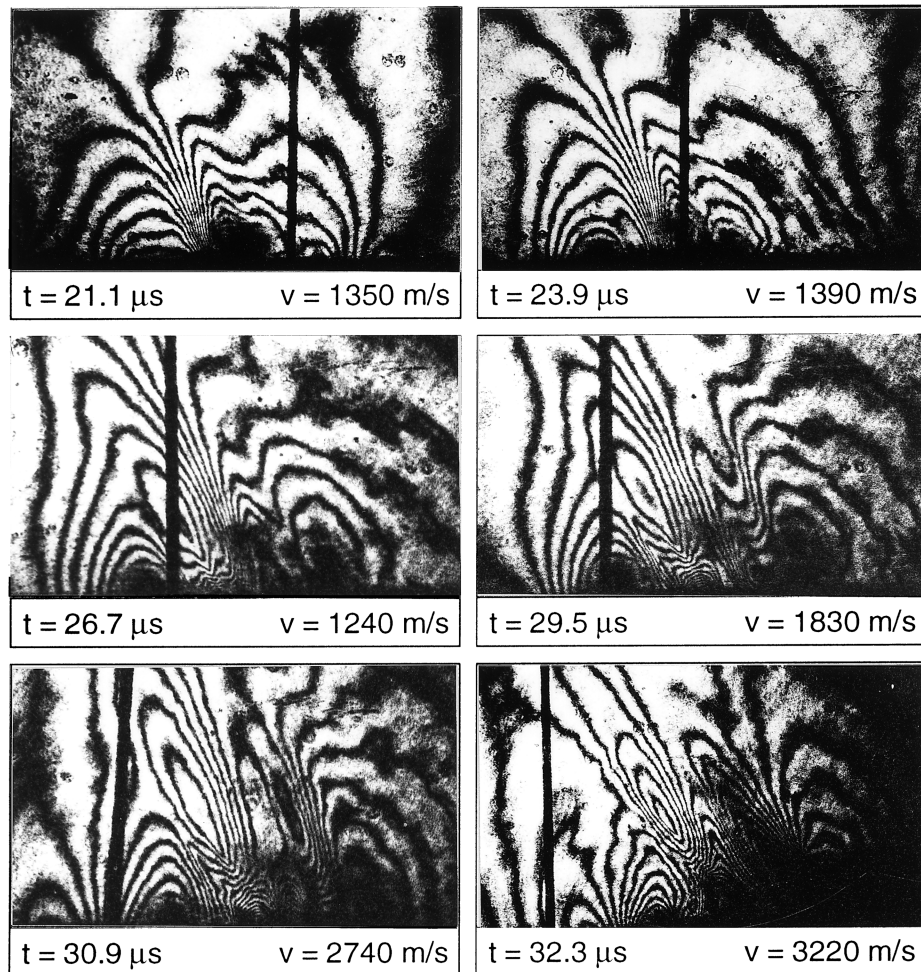


Fig. 18. Typical set of CGS interferograms obtained for dynamic crack growth along a PMMA/aluminum bimaterial interface subjected to impact loading. (Extended time window of observation.)

### CLOSURE

This paper describes experimental observations of various phenomena characteristic of dynamic intersonic decohesion of bimaterial interfaces. The optical techniques of coherent gradient sensing (CGS) interferometry and photoelasticity, were employed in conjunction with high speed photography, in separate yet complementary experiments, to explore intersonic interfacial crack propagation in two different bimaterial systems, namely, PMMA/steel and Homalite-100/aluminum.

Using the two techniques the nature of large-scale contact and mach wave formation at the vicinity of running cracks in the two bimaterial systems is explored. It is confirmed that large-scale contact does indeed occur when the crack tip speed is in

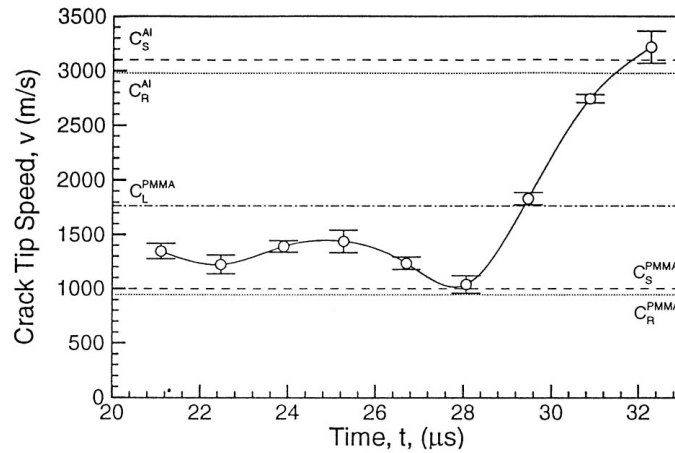


Fig. 19. Crack tip speed history of dynamic crack growth along a PMMA/aluminum bimaterial interface.

the  $c_s < v < \sqrt{2}c_s$  regime, as implied theoretically. Also, direct visual evidence is obtained for mach waves emanating from the intersonically moving crack tip and the end of the intersonically moving contact zone. In view of these experimental observations, a physical model for intersonic crack propagation along bimaterial interfaces was presented and ratified in view of recent theoretical developments. Finally, very recent experimental evidence was presented to demonstrate the possibility of super-sonic crack growth along a bimaterial interface.

#### ACKNOWLEDGEMENTS

The authors would like to acknowledge the support of the National Science Foundation through a joint Grant No. CMS-9424113 to the University of Rhode Island and the California Institute of Technology (Dr O. Dillon, Scientific Officer). A. J. Rosakis would also like to acknowledge the support of the Office of Naval Research under Grant No. N00014-95-1-0453 (Dr Y. Rajapakse, Scientific Officer).

#### REFERENCES

- Aleksandrov, V. M. and Smetanin, B. I. (1990) Supersonic cleavage of an elastic strip. *PMM U.S.S.R.* **54**(5), 677–682.
- Archuleta, R. J. (1982) Analysis of near-source static and dynamic measurements from the 1979 Imperial Valley earthquake. *Bull. Seismological Soc. Am.* **72**(6), 1927–1956.
- Broberg, K. B. (1960) The propagation of a Griffith crack. *Ark. Fys.* **18**, 159.
- Broberg, K. B. (1985) Irregularities at earth-quake slip. *J. Tech. Phys.* **26**(3–4), 275–284.
- Broberg, K. B. (1989) The near-tip field at high crack velocities. *International Journal of Fracture* **39**(1–3), 1–13.

- Burridge, R. (1973) Admissible speeds for plane-strain shear cracks with friction by lacking cohesion. *Geophys. J. R. Soc. Lond.* **35**, 439–455.
- Burridge, R., Conn, G. and Freund, L. B. (1979) The stability of a rapid mode II shear crack with finite cohesive traction. *J. Geophys. Res.* **85**(B5), 2210–2222.
- Bykovtsev, A. S. and Kramarovskii, D. B. (1989) Non-stationary supersonic motion of a complex discontinuity. *PMM U.S.S.R.* **53**(6), 779–786.
- Curran, D. R., Shockey, D. A. and Winkler, S. (1970) Crack propagation at supersonic velocities, II. Theoretical model. *Int. J. Fract.* **6**(3), 271–278.
- Dally, J. W. and Riley, W. F. (1991) *Experimental Stress Analysis*. McGraw-Hill.
- Freund, L. B. (1979) The mechanics of dynamic shear crack propagation. *J. Geophys. Res.* **84**(B5), 2199–2209.
- Freund, L. B. (1990) *Dynamic Fracture Mechanics*. Cambridge University Press, Cambridge.
- Georgiadis, H. G. (1986) On the stress singularity in transonic shear crack propagation. *International Journal of Fracture* **30**(3), 175–180.
- Georgiadis, H. G. and Barber, J. R. (1993) Steady-state transonic motion of a line load over an elastic half-space: the corrected Cole/Huth solution. *Journal of Applied Mechanics* **60**, 772–774.
- Huang, Y., Liu, C. and Rosakis, A. J. (1996) Transonic crack growth along a bimaterial interface: an investigation of the asymptotic structure of near-tip fields. *International Journal of Solids and Structures* **33**(18), 2625–2645.
- Huang, Y., Wang, W., Liu, C. and Rosakis, A. J. (1997) Intersonic interfacial crack growth in a bimaterial: an investigation of crack face contact. *Journal of the Mechanics and Physics of Solids*, in press.
- Lambros, J. and Rosakis, A. J. (1995a) Dynamic decohesion of bimaterials: experimental observations and failure criteria. *International Journal of Solids and Structures* **32**(17/18), 2677–2702.
- Lambros, J. and Rosakis, A. J. (1995b) On the development of a dynamic decohesion criterion for bimaterials. *Proceedings of the Royal Society of London*.
- Lambros, J. and Rosakis, A. J. (1995c) Shear dominated transonic interfacial crack growth in a bimaterial—I. Experimental observations. *Journal of the Mechanics and Physics of Solids* **43**(2), 169–188.
- Liu, C., Huang, Y. and Rosakis, A. J. (1995) Shear dominated transonic interfacial crack growth in a bimaterial—II. Asymptotic fields and favorable velocity regimes. *Journal of the Mechanics and Physics of Solids* **43**(2), 189–206.
- Liu, C., Lambros, J. and Rosakis, A. J. (1993) Highly transient elastodynamic crack growth in a bimaterial interface: higher order asymptotic analysis and experiments. *Journal of the Mechanics and Physics of Solids* **41**(12), 1887–1954.
- Rice, J. R. (1988) Elastic fracture mechanics concepts for interfacial cracks. *Journal of Applied Mechanics* **55**, 98–103.
- Rosakis, A. J. (1993) Two optical techniques sensitive to gradients of optical path difference: the method of caustics and the coherent gradient sensor (CGS). *Experimental Techniques in Fracture*, pp. 327–425.
- Rosakis, A. J., Samudrala, O. and Singh, R. P. (1997) Work in progress. Graduate Aeronautical Laboratories, California Institute of Technology, Pasadena, California.
- Singh, R. P. and Shukla, A. (1996) Subsonic and intersonic crack growth along a bimaterial surface. *Journal of Applied Mechanics* **63**, 919–924.
- Singh, R. P., Lambros, J., Shukla, A. and Rosakis, A. J. (1997) Investigation of the mechanics of intersonic crack propagation along a bimaterial interface using coherent gradient sensing and photoelasticity. *Proceedings of the Royal Society of London*, in press.
- Tippur, H. V. and Rosakis, A. J. (1991) Quasi-static and dynamic crack growth along bimaterial interfaces: a note on crack-tip field measurements using coherent gradient sensing. *Expt. Mech.* **31**(3), 243–251.
- Tippur, H. V., Krishnaswamy, S. and Rosakis, A. J. (1991) A coherent gradient sensor for crack tip measurements: analysis and experimental results. *International Journal of Fracture* **48**, 193–204.

- Winkler, S., Shockey, D. A. and Curran, D. R. (1970) Crack propagation at supersonic velocities, I. *International Journal of Fracture* **6**(2), 151–158.
- Xu, X.-P. and Needleman, A. (1996) Numerical simulations of dynamic crack growth along an interface. *International Journal of Fracture* **74**, 289–324.
- Yang, W., Suo, Z. and Shih, C. F. (1991) Mechanics of dynamic debonding. *Proceedings of the Royal Society of London* **A433**, 679–697.